Heliyon 10 (2024) e34795

Contents lists available at ScienceDirect

Heliyon

journal homepage: www.cell.com/heliyon

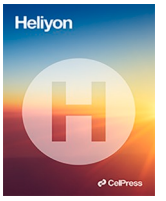

Review article

Optimizations of luminescent materials for white light emitting diodes toward healthy lighting

Fen Wang [a], Hao Pan [b], Wei Mao [c], Dan Wang [a,*]

[a] State Key Laboratory of Organic-Inorganic Composites, Beijing University of Chemical Technology, Beijing, 100029, China
[b] Shandong Best Integrated Housing Co., Ltd, Weifang, 262600, China
[c] Quzhou Innovation Institute for Chemical Engineering and Materials, Quzhou, 324000, China

ARTICLE INFO

Keywords:
wLEDs
Healthy lighting
Luminescent materials
Phosphors

ABSTRACT

White light emitting diodes (wLEDs) have been widely used as the green lighting sources. The commercial wLEDs devices are mainly achieved through the combination of blue emission chips and yellow phosphors, which offer advantages of high efficiency and long lifetime. However, the color rendering index (CRI) of traditional wLEDs is low due to the lack of red components. In recent years, with the improvement of the quality of life, a lot of efforts have been paid to improve the performance of wLEDs devices related to CRI, correlated color temperature, light uniformity, luminous flux, etc. In this article, we summarize the recent advances on the optimization of wLEDs toward healthy lighting. Brief introductions on the fundamentals of healthy effect of lighting are presented, followed by discussions of current methods to realize wLEDs devices. Special overviews on strategies for luminescent materials of wLEDs in recent years are presented. The opportunities and challenges in the future development of wLEDs lighting devices are also discussed.

1. Introduction

White light emitting diodes (wLEDs) are becoming the most popular lighting devices around the world, which are typically fabricated by blue emission chips with rare-earth doped phosphors with yellow emission under the excitation of blue light to produce white light [1–3]. Compared with previously used lighting devices such as incandescent and fluorescent bulbs, wLEDs use less energy with no glass or mercury, negating the risk of glass shards or toxic metal floating which have been regarded as the direction of future lighting [4]. For example, it is forecast that LEDs will penetrate around 86 % of electrical lighting installations by 2035 in the United States [5]. The popularity of electrical lighting has also put people's attention on the environmental impacts of the artificial light at night itself [6]. Human's biological clock controlling circadian rhythms have been changed for increasing reliance on artificial lighting found in existing studies [7]. Apart from that, too much blue light and the lack of red light in the light source will lead to poor color rendering of the light. The original color of the object can't be presented, which can easily lead to visual fatigue, and will also affect people's mood and appetite to a large extent. Besides, human visual perception depends on the regulation of pupil and photoreceptor cells. The pupil adjusts its size according to the strength of the external light to make the luminous flux on the retina remains moderate. Therefore, when the eyes are in uneven light for a long time, it will make the eyes tried, and to a certain extent, it will destroy the photosensitive cells on the retina, so that vision is affected. In view of the impact of light source on human health, there is an urgent

* Corresponding author.
E-mail address: wangdan@mail.buct.edu.cn (D. Wang).

https://doi.org/10.1016/j.heliyon.2024.e34795
Received 19 March 2024; Received in revised form 27 June 2024; Accepted 17 July 2024
Available online 17 July 2024

need to improve light quality. In this paper, we introduce the influence on health of artificial light, current fabrication methods of wLEDs, analyze its advantages and disadvantages, list the performances of healthy light source and summarize the optimization strategies for the most commonly used wLEDs at present, and put forward the prospect of the future lighting.

2. Fundamentals of healthy lighting

2.1. Visual effect of lighting

Ambient lighting is vital for visual health of human eye, including the spectral composition and intensity of light. There is increasing evidence that the spectral composition of ambient lighting can influence normal ocular growth and refractive development and the intensity of ambient lighting has a great influence on the ciliary muscle because it needs to adjust focal distance and light exposure according to luminance of lighting environment. The impact of the spectrum on visual health can't be underestimated. Infant rhesus monkeys were used as experimental subjects to draw a conclusion that the long-wavelength red light greatly reduced the likelihood of developing either form-deprivation myopia or compensating myopic changes in response to imposed hyperopic defocus [8]. Besides, it has been preliminarily demonstrated that 650 nm low-level red light not can slow down myopia progression, but also reverses the myopia progression in human [9,10]. In contrast, short-wavelength blue light may lead to retinal damage and degeneration and the primate threshold of phototoxicity for wavelength between 400 and 450 nm was experimentally fixed at 22 J/cm^2 [11–13]. At the same time, a lighting environment with suitable luminance is also needed for visual health. More consumption of strength is needed from ciliary muscle adjusting light exposure to obtain clear image in retina in dark ambient lighting contributing to visual fatigue. [2,14] Further experiments imply that luminance above 80 cd/m^2 would be helpful to prevent the accumulation of visual fatigue [15].

2.2. Non-visual biological effect of lighting

Apart from a visual effect, light entering the human eyes has also an important non-visual biological effect on the human body [16–18], which is mediated by the non-image-forming intrinsically photosensitive retinal ganglion cells (ipRGCs) in the retina [19,20]. These effects are manifested in changes in sleep behavior [21,22], alertness [17,18,21], mood [18–20]. A third type of light-sensitive cells unlike cone and rod photoreceptors, ipRGCs, can affect the circadian phase by reporting light stimuli to the suprachiasmatic nucleus (SCN) to slow down the melatonin secretion, which have spectral sensitivity to light in the blue part around 460–480 nm [19,22] The circadian stimulus value increases with corneal illumination and decreases with correlated color temperature (CCT) in a certain range and the artificial lighting with the CCT of 2700 K and 4000 K can be selected to reduce the impact on circadian phase [22]. The ipRGC-driven effects and mechanisms of light on mood have been studied [20,23]. The means of positive mood always decreased with an increase in CCT [24]. Multiple studies have proven that lighting environment with CCT of 4000 K is beneficial for both circadian phase and mood (Fig. 1) [19,24].

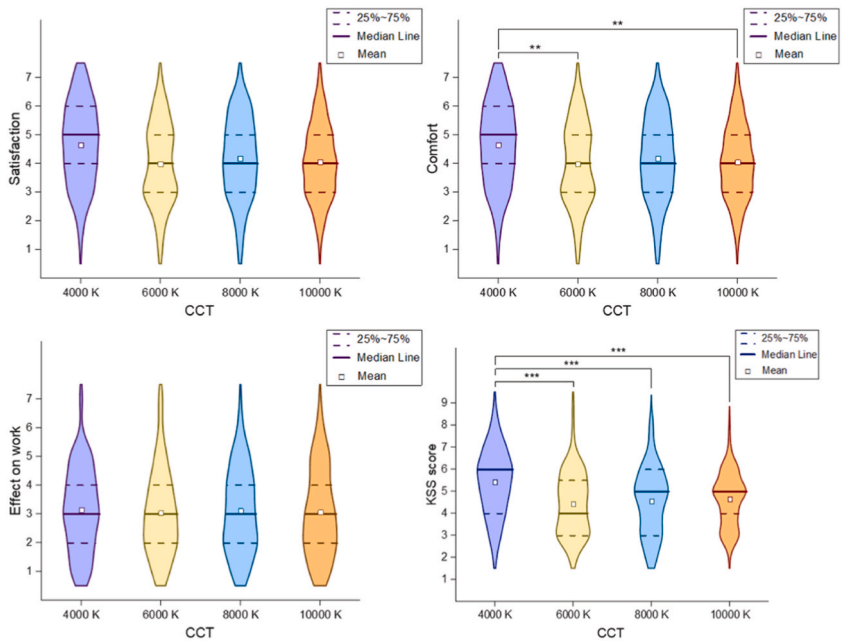

Fig. 1. The distributions of the subjective perception feedback (Reprinted with permission from Ref. [24], copyright 2022, Elsevier).

3. Product features of wLEDs

There are several parameters to evaluate the characteristics of ambient lighting, including CCT, color rendering index (CRI), CCT uniformity, luminous flux, etc. Among them, CCT and CRI are mainly affected by the spectral composition of light. Luminous flux defines the light emitted by a source such as a lamp or received by a surface, irrespective of direction, which can measure the intensity of light. Light uniformity refers to whether the spectral composition and intensity of light are consistent at different angles. It is generally accepted that the spectral composition and intensity of light have a huge impact on body's health, so a suitable light can be selected according to these parameters to achieve healthy lighting. CRI represents the ability of a light source to accurately reproduce the color of the object it illuminates. When there is little or no main wave reflected by the object under the reference light source in the light source spectrum, the color will produce a significant chromatic difference. The CRI of sunlight is defined as 100, and the larger the CRI, the closer to the natural light source [25]. CCT is an important measurement standard of wLEDs products, which is related to the color characteristics of wLEDs light source display [26]. The more blue-components in the emission spectrum of lighting source, the higher CCT. CCT uniformity is one of the major problems in wLEDs fabrication, which is associated with the different ratios of blue and yellow emissions, leading to different CCTs at various angles. As a result, there is a yellow ring phenomenon in the application of wLEDs bring a poor lighting experiments [27]. Besides, in the process of the light emitted from the chip through the encapsulating material layer into the air, there are total reflection at the interface reduce the light extraction efficiency and the luminous flux because the difference of refractive index (RI) between semiconductor chips (>2.4 for blue chips of gallium nitride) and encapsulating materials (1.5–1.6 for commercial silicone) [28]. From the point of view of human health and energy saving, we need a white lighting source with high CRI, low CCT, uniform light output and high luminous flux.

Commercial wLEDs are usually approached by integrated packaging of a diode generating a short wavelength and phosphors absorbing a few short wavelength photons and converting them into longer wavelength photons, because white light sensation can be caused when two photons of complementary wavelengths arrive simultaneously on the human eye (Fig. 2a) [2,11,29–32]. The advantages of this combination is that it is simple to make and has the lowest cost and highest efficiency among all the combinations of wLEDs. The efficiency of this kind of wLED is affected by both LED chips and phosphors. Low CRI and high CRI is the biggest deficiency of the wLEDs realized by combining the blue LED and YAG:Ce, mainly caused by the weak luminosity of the phosphor in the red region, and more blue light of short wavelengths than a sunset, originating in narrowband blue-light emission from a semiconductor LED. Apart from that, wLEDs can be composed of ultraviolet LED (UV-LED) chip and phosphors with different color (Fig. 2b) [33,34]. The principle of white lighting is that UV-LED pump different phosphors emitting red, green, blue lights respectively, and the white light can be obtained by adjusting the ratio of three phosphors. Because UV light will not participate in the composition of white light, it is much simpler than blue LED to control the color and the higher CRI and lower CCT can be obtained. But the low efficiency of UV-LED which drops dramatically at wavelengths below 400 nm limits its commercialization, and because the energy difference between the excited and emitted photons is a natural energy loss, when UV light is converted to red, its energy loss is 10 %–20 % higher than that when it is converted from blue light. There is color reabsorption between the mixtures of different phosphors, and it is difficult to match the absorption wavelength of the tricolor phosphor with the emission wavelength of its LED at the same time, which will have a greater impact on lumen efficiency and CRI. What's more, the uneven grain size and specific gravity (affecting settling velocity) of phosphors make inhomogeneous color and intensity distribution in the whole system, which also reduces the conversion efficiency of phosphors. Another way of wLEDs implementation is to combine red LED, green LED and blue LED chips into a pixel to achieve white light (Fig. 2c). This way can control the LEDs with different color separately, leading to a high flexibility of color adjustment and can obtain an ideal light source. Besides, the color purity of white light obtained by this way is also high, so this wLED has a huge market potential in large liquid crystal display (LCD) backlight. But the three colors need to be compensated with feedback circuits to keep the light stable, so that the production cost of white light synthesized by this method is the highest. Table 1 summarize the characteristics

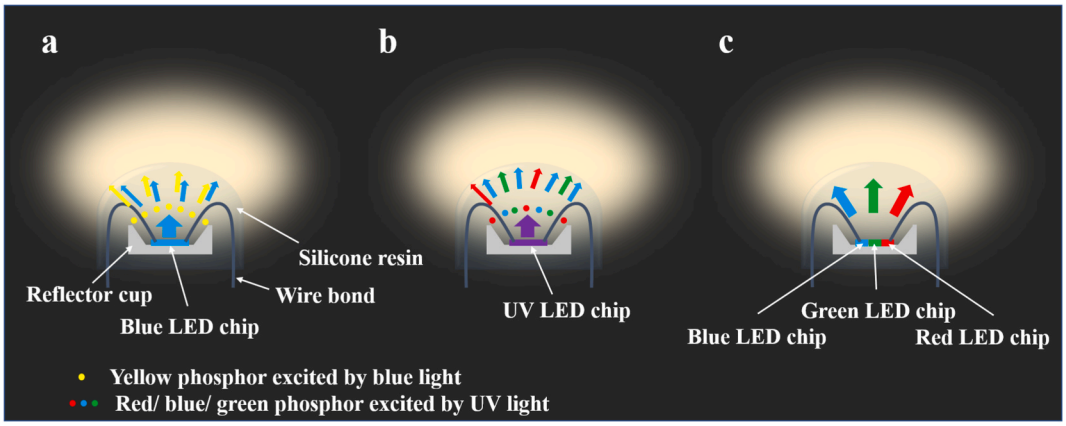

Fig. 2. Three approaches to relized wLEDs for lighting. a) wLED composed of blue LED chip and yellow phosphors, b) wLED composed of UV-LED chip and phosphors with different color, c) wLED composed of three-primary color LED chips. (For interpretation of the references to color in this figure legend, the reader is referred to the Web version of this article.)

of three types wLEDs. In general, the most mature method at present is the combination of 460 nm blue InGaN chip and yellow light YAG:Ce phosphor into wLEDs. In view of the problems existing in this combination, optimizing the phosphor to improve the quality of lighting sources and actively exploring new phosphor to replace YAG:Ce is one of the main topics in the current research and development of wLEDs.

4. Optimization Strategies of wLEDs

4.1. Tuning the emission spectrum of phosphors

Typical unit of wLEDs consists a blue emission chip with a certain amount of yellow luminescent particles encapsulated in packaging materials. As key materials for tuning the emission spectra of wLEDs, luminescent particles are supposed to have the following characteristics: a) excitation spectrum exhibits well overlap with emission of blue LED chip in the wavelength region of 420–480 nm, b) high stability under practical application conditions such as oxygen, carbon dioxide, chemical reagents, water and thermal treatment, c) emission spectra with suitable CRI and CCT when combined with blue light of the chip, d) the luminescent materials can be synthesized in mild conditions, including easy control of particle morphology, harmless production and reasonable cost. To date, many kinds of luminescent materials have been studied for wLEDs, including carbon dots [35–40], semiconductor quantum dots [30,31,41], and inorganic phosphors [1,42–44]. Among them, luminescent ions doped inorganic crystals are most commonly used luminescent materials in LED lighting, which can make white light softer, improve the color reproduction and light efficiency of devices. Tuning the emission spectrum of light is an effective method to improve the CRI and reduce CCT, includes doping modification of phosphors to make the original yellow phosphor emission wavelength redshift to increase the red component [45], or adding an appropriate amount of red phosphor to the yellow phosphor to improve the CRI [41]. As shown in Table 2, the CRI is significantly improved after the addition of red components, and it can also be seen that, compared with optimizing the existing yellow luminescent materials, directly adding red phosphors has a more obvious effect on reducing the value of CCT, which less than 4000 K beneficial for both circadian phase and mood.

4.1.1. Yellow-emitting phosphors pumped by blue LED

Ordinary products of wLEDs are approached by integrated packaging of blue chips made of GaN and luminescent particles of YAG:Ce.[1] The space group of $Y_3Al_5O_{12}$(YAG) belonging to cubic crystal system is *Ia3d*, and YAG exhibits excellent optical and thermodynamic performance. Y in the dodecahedral sites has an ionic radius similar to that of most rare earth elements and is easily substituted. In case of doping with Ce^{3+}, the Ce ions occupy Y resulting in a shift of Ce^{3+}'s 5d-4f emission corresponding to yellow-green spectral region. People's eyes and brain work together to blend human perception of separate bands of blue color from chips and yellow color from phosphors into a white light that may be illuminating the object viewed [7,51]. In order to improve the light source quality of wLEDs based on YAG:Ce, many efforts have been paid optimize the luminescent center ion and the structure of host. For instance, the YAG, can be written as $A_3B_2C_3O_{12}$, where A, B, and C represent three different lattice positions, and the intensity crystal field strength in the dodecahedral sites of YAG directly depends on the R^{3+}-O^{2-} cation–anion distances. As the ionic radius of R^{3+} increases, the corresponding cation–anion distances become smaller, and the crystal field strength is larger [52–55]. As shown in Fig. 3a and b, the substitution of Gd^{3+} for Y^{3+} results in red shift by increasing the crystal field splitting effect for the ionic radius of Gd^{3+} (0.1053 nm) is larger than that of Y^{3+} (0.1019 nm) [56,57]. Similarly, the substitution of Tb^{3+} with larger ionic radius (0.104 nm) for Y^{3+} can play a similar role in tuning the emission spectrum of light [54,55]. The above way only substitute cations in single-site, and there are other way to substitute cations is double-site substitution. The existed research has demonstrated that when Mg^{2+}–Si^{4+}/Ge^{4+} as ion pairs substituting for $Al(1)^{3+}$– $Al(2)^{3+}$ are synchronously incorporated into the YAG:Ce host lattice, the 5d level is lowered, and the emission peak shifts to longer wavelength [50,58,59]. However, the sites of substitution are disputed, and there are another theory that the Y^{3+}-Al^{3+} are substituted by M^{2+}-Si^{4+} (M = Ba, Sr, Ca, Mg), and red-shift increases with the decrease of M^{2+} radius [60]. But one thing is certain, that is, the Ce^{3+}–O^{2-} bond length is decreased, resulting in redshift according to the following equation:

$$D_q = \frac{1}{6} Ze^2 \frac{r^4}{R^5} \tag{1}$$

where Dq is a measure of the energy level separation, Z is the anion charge, e is the electron charge, r is the radius of the d wavelength, and R is the bond length [58]. Interestingly, interstitial defects caused by carbon atoms also can shorten the Ce^{3+}–O^{2-} bond length,

Table 1
Characteristics of three types wLEDs.

Feature	Blue LED + yellow phosphor	UV-LED + RGB phosphor	RGB LED
CRI	Moderate	High	High
CCT	High	Low	Low
CCT uniformity	Low	High	Low
Structure	Simple	Simple	Complicated
Cost	Low	Low	High
Efficiency	High	Low	High

Table 2
Typical luminescent materials and its devices.

Strategy	Materials	Emission/nm	wLED performance		Reference
			CCT/K	CRI	
Adding red-emitting materials	$Cs_2NbOF_5:Mn^{4+}$	631.5	3168	90	[46]
	$Li_3Na_3Al_2F_{12}:Mn^{4+}$	629	3874	90.6	[2]
	$K_2TiF_6:Mn^{4+}$	580–660	2736	87.3	[43]
	$K_3TaO_2F_4:Mn^{4+}$	630	3488	90.0	[47]
	$SrLiAl_3N_4:Eu^{2+}$	650	2875	91.1	[48]
	CD	620	3827	92.7	[29]
Optimizing yellow-emitting materials	$Ca_4SiAl_3N_7:Ce^{3+}$	568	4068	89.6	[49]
	$Ce:Y_{2.99}(Mg_xAl_{5-2x}Si_x)O_{12}$	571	4384	81	[50]
	$CaY_2Al_4SiO_{12}:Ce^{3+},Mn^{2+}$	543, 616, 750	5460	90.5	[45]

leading to a larger crystal field splitting of 5d orbital of the Ce^{3+} atom and bigger 5d centroid shift [61].

Based on the energy transfer from Ce^{3+} to red light emitting activators, such as Mn^{2+} [45,62,63], Pr^{3+} [64],Cr^{3+} [65], etc., can also supplement the red component of the spectrum. Mn^{2+} is a common red-light emitting activator, the energy transfer process is briefly described with the example of Mn^{2+}. As shown in Fig. 3c and d, the energy transfer process can achieve from Ce^{3+} to neighboring Mn^{2+} via non-radiation transition because the lowest 5 d^1 energy level of Ce^{3+} is a little higher than the $^4T_1$ of Mn^{2+}. And then the $^4T_1$ excited electrons transfer back to $^6A_1$ ground state, which emits three bands at 528, 590, and 745 nm supplementing the red light, and the CCT of wLED can decrease from 4044 K to 3152 K [63].

In addition, phosphors with nitride as hosts are promising candidates for wLED [42,49,66]. These materials mainly are obtained by introducing N into the crystal structure of silicates or aluminosilicates, which can meet the needs of wLED for color conversion, because their coordination environment with strong rigidity, diverse structure and high covalency can reach strong absorption of blue light and long wavelength emission and high-quantum efficiency [49]. As reported, some phosphors belonging to nitridosilicate and nitridoaluminosilicate, such as $Ca_{8-x}Mg_7Si_9N_{22}:xCe^{3+}$ [42], $(La,Ca)_3Si_6N_{11}:Ce^{3+}$ [67], $Ca_4SiAl_3N_7:Ce^{3+}$ [49], $Ba_5Si_{11}Al_7N_{25}$: Eu^{2+} [66], can be effectively excited by the blue chip and emit a strong broadband yellow light. $Ca_4SiAl_3N_7:Ce^{3+}$ has more red light components than $YAG:Ce^{3+}$ accounting for 64 %, and wLED based on it has a CRI of 89.6 and a CCT of 4068 K (Fig. 3e and f) [49]. Compared with the PL spectrum of $YAG:Ce^{3+}$, the $Li_2SrSi_2N_4:Ce^{3+}$ spectrum shows a broader emission band due to the two sites in $Li_2SrSi_2N_4$ for Ce^{3+} to occupy reflected in Fig. 3g and h [68]. Apart from excellent optical performances, the thermal stability of these phosphors can meet requirement of wLEDs due to the highly condensed three-dimensional network structure based on $Si(Al)N_4$ tetrahedra and the stable chemical bonding between the atoms. $Ba_5Si_{11}Al_7N_{25}$: Eu^{2+} phosphor, as an example, can remain >90 % of the initial intensity at 83 K at 473 K and the quenching temperature is about 700 K [66]. But the harsh synthesis condition requiring high temperature and pressure, hinders its development progress. It is key to explore phosphors with nitride as hosts phosphors that can be synthesized at lower temperature and atmospheric pressure with high efficiency and stable emission.

4.1.2. Red-emitting phosphors pumped by blue LED

Adding red phosphor excited by blue light is a direct and effective way to supplement the red component of wLED light, which can also reduce CCT and improve CRI [2,71]. Therefore, the study of red phosphor for wLED has attracted extensive attention in recent years. Eu^{2+} and Mn^{4+} are the most commonly used red luminous centers. A comparison of some recently reported red-emitting phosphors is shown in Table 3. The first generation of red phosphors are Eu^{2+} activated sulfides represented by CaS and SrS [72]. Although they can make up for the deficiency of red light, these sulfide phosphors cannot be commercialized because they are hygroscopic and will produce toxic gases during the hydrolysis process. At present Eu^{2+} doped nitride phosphors are the most mature red materials with high quantum efficiency and high quenching temperature [73]. Compared with the traditional oxide matrix, the nitride matrix has a more excellent effect in rearranging electron cloud, which can split the 5d energy level, ultimately leading to a smaller 4f-5d energy level difference to achieve a better match between phosphors and blue LED chips (Fig. 4a–c) [74]. However, the preparations of nitride phosphors are in harsh conditions, usually requiring high temperature >1700 °C and high pressure >0.9 MPa [75]. Mn^{4+}, a transition metal ion, has been regarded as a promising red emission luminescence center, which is doped in oxides [76], fluorides [2,44,77] and oxyfluoride [46,47] matrix to obtain red phosphors showing good luminescence properties and playing an important role in improving the CRI of wLEDs. The ground state energy level of Mn^{4+} is $^4A_2$. When it is excited, $^4A_2$ transitions to excited states including $^4T_1$ and $^4T_2$, and then produces $^2E \rightarrow {}^4A_2$ radiation transitions, which lead to red emission (Fig. 4d–f). Fluoride matrix with Mn^{4+} doping has the characteristics of mild synthesis conditions, low crystallization temperature, and strong absorption of blue light. And $K_2SiF_6:Mn^{4+}$ and $K_2TiF_6:Mn^{4+}$ as the typical example, have been commercialized [32,46]. However, toxic hydrofluoric acid is used in the preparation process, and the phosphor is unstable in high humidity environment. After water absorption, decomposition reaction will generate MnO_2 covering phosphors and toxic HF gas as follows, which reduces the color stability of wLEDs and pollute the environment [44]. Some researchers focused on improving the water resistance of phosphors, including surface coating to isolate water [43,77], or optimizing the crystal field of matrix to improve the stability of Mn^{4+} [44]. As shown in Fig. 4g, a Mn^{4+}-activated fluoride red phosphor, $K_2TiF_6:Mn^{4+}$(KTF), moisture resistance of which became better after superhydrophobic surface modification with octadecyltrimethoxysilane, can maintain at 83.9 % or 84.3 % of luminous efficiency after being dispersed in water for 2 h or aged at high temperature (358 K) and high humidity (85 %) atmosphere (HTHH) for 240 h, respectively. The moisture resistance can also be optimized from the perspective of crystal field of matrix. For example, the moisture and thermal stability of

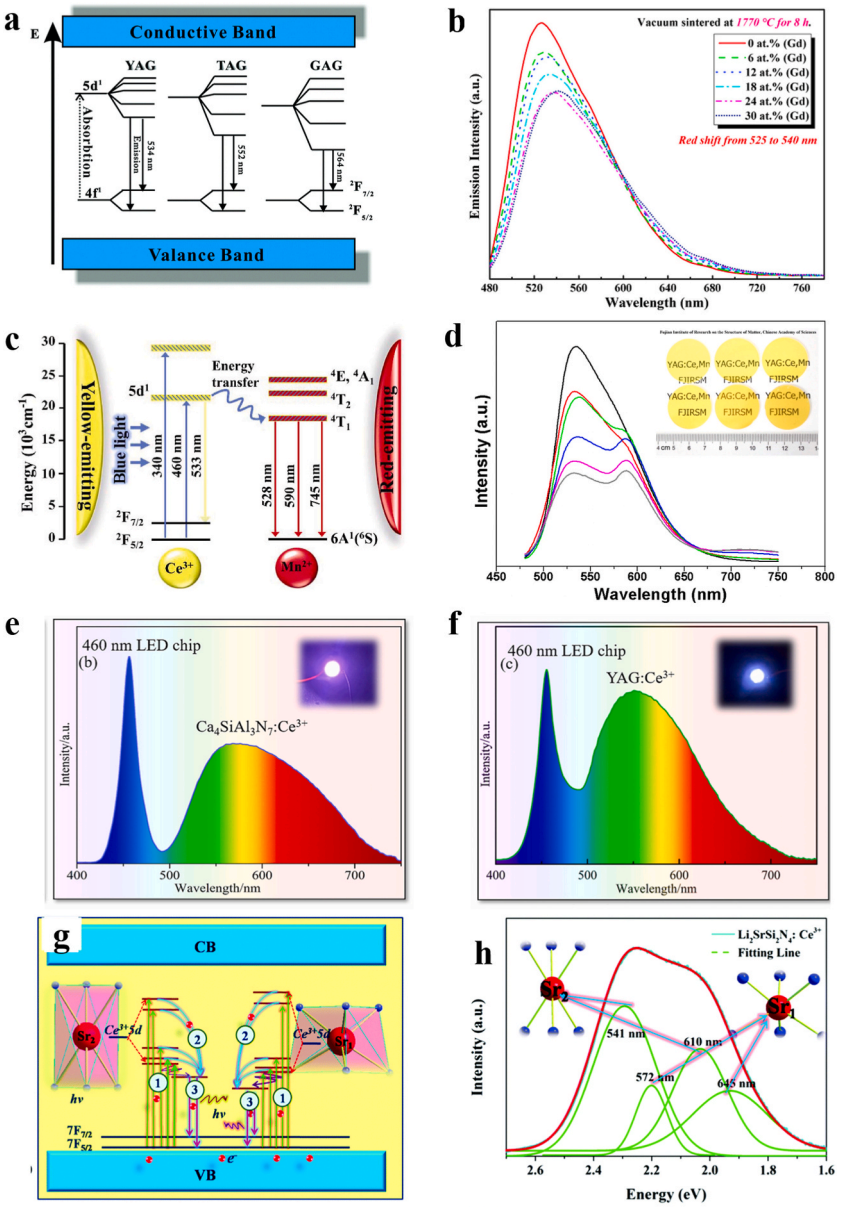

Fig. 3. a) Schematic energy diagram of Ce^{3+} in YAG, TAG, and GAG (Reprinted with permission from Ref. [69], copyright 2017, Royal Society of Chemistry), b) emission spectra of Ce:(Y,Gd)AG ceramics with different Gd^{3+} ions substitution (Reprinted with permission from Ref. [70], copyright 2019, Elsevier), c) schematic illustration of the energy transfer process in YAG:Ce,Mn, d) PL spectra of YAG:Ce,Mn under 460 nm excitation (Reprinted with permission from Ref. [63], copyright 2020, Junrong Ling et al.), e,f) EL spectrum of $Ca_4SiAl_3N_7:Ce^{3+}$ based WLED(e) and YAG:Ce^{3+} based WLED(f) with 460 nm blue LED chip as excitation source (Reprinted with permission from Ref. [49], copyright 2023, Elsevier), g,h) the energy level diagram(g) and the Gaussian peaks fitting for PL spectrum(h) of Ce^{3+}-doped $Li_2SrSi_2N_4$ phosphor (Reprinted with permission from ref. [66], copyright 2018, Royal Society of Chemistry). (For interpretation of the references to color in this figure legend, the reader is referred to the Web version of this article.)

$K_2Ge_{0.6}Ti_{0.4}F_6:Mn^{4+}$ under cation substitution can keep 71 % or 83 % of the original luminescence intensity after immersing in deionized water for 180 min or treated under 423 K, and a wLED with high CRI of 92.4, low CCT of 3113 K and high luminous efficiency of 123.1 lm/W can be obtained by encapsulating it with commercial yellow phosphors on blue chip [44]. In that work, the mechanism was explained that the moisture stability of phosphors are significantly enhanced under the synergistic effects of the two following reasons: the expanded unit cell caused elongation of Mn–F bond by substituting the Ge^{4+} (r = 0.53 Å) site with Ti^{4+}(r = 0.60 Å) promotes the dissociation of $[MnF_6]^{2-}$ and then enhance the reaction between $[MnF_6]^{2-}$ and H_2O (Fig. 4h), meanwhile, the complex with inner orbital hybridization $[TiF_6]^{2-}$ based on the six empty d^2sp^3 hybridization orbitals is more stable than that of the outer orbital hybridization $[GeF_6]^{2-}$ based on the six empty sp^3d^2 hybridization orbitals. In recent years, developing novel green

Table 3
Typical red phosphors.

Light Emitting Activators	Host	Materials	Excitation /nm	Emission /nm	Reference
Mn^{4+}	Oxyfluoride	$Cs_2NbOF_5:Mn^{4+}$	467	631.5	[46]
		$K_3TaO_2F_4:Mn^{4+}$	360, 460	630	[47]
		$LiAl_4O_6F:Mn^{4+}$	150–550	662	[81]
	Fluoride	$Li_3Na_3Al_2F_{12}:Mn^{4+}$	467	629	[2]
		$K_2TiF_6:Mn^{4+}$	462	580–660	[43]
		$K_2Si_{1-x}F_6:xMn^{4+}$	450	630	[78]
		$Na_3GaF_6:Mn^{4+}$	467	626	[82]
		$K_2LiAlF_6:Mn^{4+}$	300–500	635	[83]
	Oxides	$CaAl_2Si_2O_8:Mn^{4+}$, Mg^{2+}	330	652	[76]
		$SrMgAl_{10-y}Ga_yO_{17}:Mn^{4+}$	340	661	[80]
		$Sr_4Al_{14-x}Ga_xO_{25}:Mn^{4+}$	450	665	[84]
		$Li_2MgTiO_4:Mn^{4+}$	476	676	[85]
Eu^{2+}	Nitride	$SrLiAl_3N_4:Eu^{2+}$	400–600	650	[48]
		$CaAlSiN_3:Eu^{2+}$	460	550–800	[86]
		$Sr_2Si_5N_8:Eu^{2+}$	421	616	[87]
	Sulfide	$(Sr,Zn)S:Eu^{2+}$	400–500	606	[88]
		$SrS:Eu^{2+}$	430–500	609	[89]

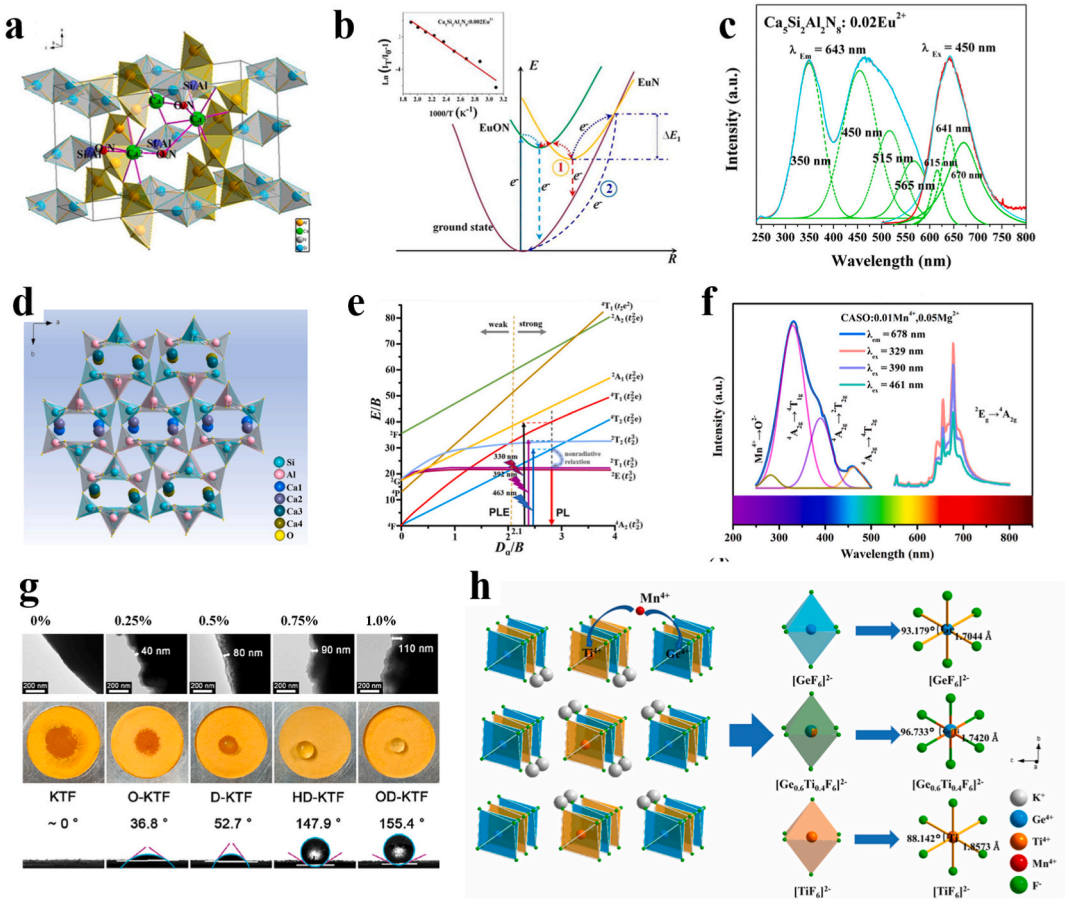

Fig. 4. a-c) The crystal structure(a), configurational coordinate diagram of the ground state of Eu^{2+} and the excited states of Eu^{2+}(b), PL and PLE spectrum(c) of $Ca_5Si_2Al_2N_8$: Eu^{2+} (Reprinted with permission from Ref. [74], copyright 2016, Elsevier), d-f) crystal structure(d), Tanabe–Sugano diagram for the 3 d^3 electron configuration of Mn^{4+}(e), PLE and PL spectra(f) of $CaAl_2Si_2O_8:Mn^{4+}$, Mg^{2+} (Reprinted with permission from Ref. [76], copyright 2023, John Wiley and Sons), g) TEM images of KTF modified and images of a drop of water on the modified KTF phosphors (Reprinted with permission from Ref. [43], copyright 2018, American Chemical Society), h) crystal structure of $K_2Ge_{1-x}Ti_xF_6:Mn^{4+}$ phosphors(Reprinted with permission from Ref. [44], copyright 2023, Elsevier).

synthetic routes for the highly efficient fluorides with Mn^{4+} doping red phosphors is also a hot spot, and the main method is to reduce the use of toxic HF by replacing it with low-toxic NH_4F/HCl or H_3PO_4/KHF_2 [32,78]. When the oxide exhibiting better chemical stability is used as matrix, the luminous color of Mn^{4+} is located in the deep red emission region, which does not match the sensitive range of human eyes. Besides, compared to fluoride phosphors, the absorption of blue light of is less effective, which can't perfectly satisfy the application for blue-excited wLEDs [79,80]. Red phosphors based on oxyfluorides not only have higher chemical stability than fluoride phosphors, but also has stronger blue light absorption than oxide phosphors [46].

4.1.3. Other frontier luminescent materials for wLEDs

In recent years, semiconductor quantum dots, metal halide perovskites, and luminescent carbon dots with high quantum efficiency, adjustable luminous color and high color saturation are also becoming substitutes for rare earth doped phosphors [30,31,41,90–96]. Semiconductor quantum dots are composed of core material enclosed within a shell of another semiconductor material with a diameter of 2–10 nm as shown in Fig. 5a and b [97]. The size of QDs reflects the properties like optical property, absorbance and photoluminescence in dependent manner. In addition, the PL emission wavelength of the ternary alloyed QDs can be tuned via adjusting the chemical composition. For example, by means of altering chemical composition, the AIS/ZnS QDs synthesized via a microwave-assisted aqueous method exhibited tunable emission ranging from 540 to 622 nm (Fig. 5c) and yellow AIS/ZnS quantum dots with high PL QY of 58.27 % were applied on commercial blue InGaN chips for wLED with a CRI of 75.6 and a CCT of 4393 K (Fig. 5d) [91].

Perovskite are organic–inorganic or all-inorganic materials with the form of ABX_3, and their electronic and optoelectronic properties are tightly related to and thus can be tuned to be ideal materials for wLED by the size, shape, surface, structure and component [98–100]. For example, $CsGeBr_3$ demonstrated the capability to emit white light under UV radiation and the device fabricated by

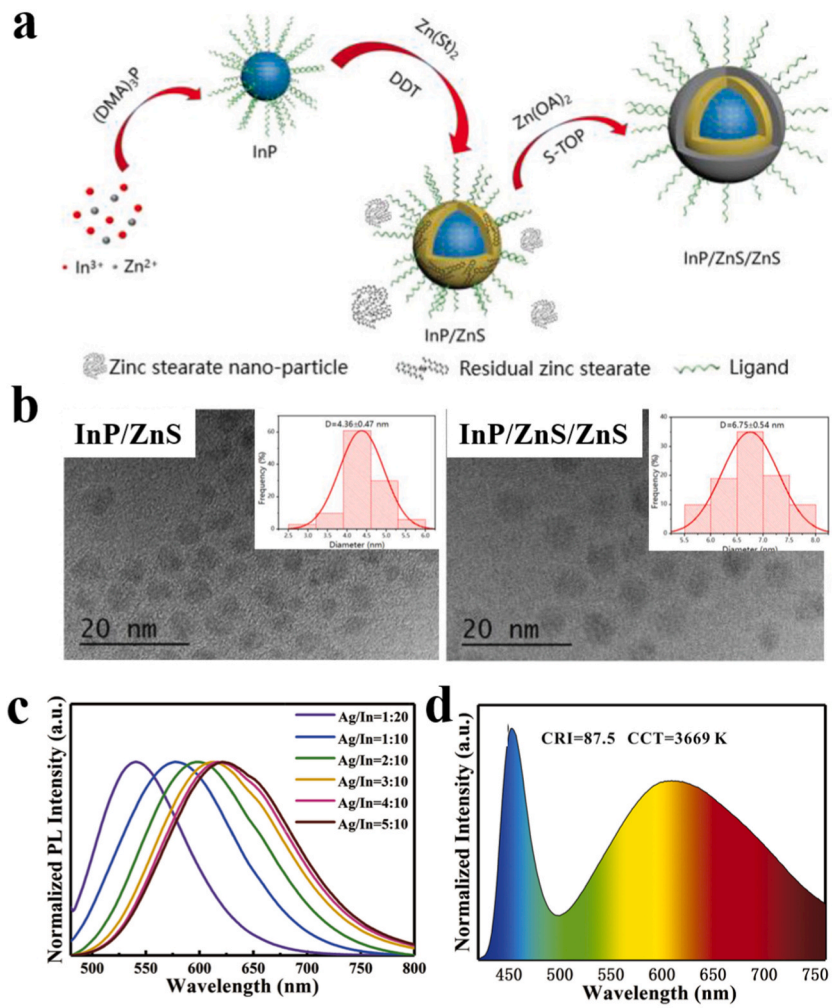

Fig. 5. a) Schematic illustration for the synthesis of thick shell InP/ZnS/ZnS QDs, b) TEM image of InP/ZnS and InP/ZnS/ZnS QDs (Reprinted with permission from Ref. [97], copyright 2020, John Wiley and Sons) c) PL spectra (λ_{ex} = 460 nm) of AIS/ZnS QDs, d) Emission spectrum of the LED based on AIS/ZnS QDs (Reprinted with permission from Ref. [91], copyright 2020, Elsevier).

$CsGeBr_3$ combined with red-emitting MOF:Eu^{3+} phosphors can exhibit a commendable CRI of 92 and a CCT of 3020 K [96]. In another work, Zhang et al. develop the synthesis of heterostructural $CsPbX_3$-PbS (X = Cl, Br, I) quantum dots via a room temperature in situ transformation route [98]. The $CsPbX_3$-PbS quantum dots show uniform size distribution as the TEM images shown in Fig. 6a and exhibit tunable dual emission feature with the visible and near-infrared photoluminescence (PL) as the PL spectra shown in Fig. 6b [98]. As one of rising stars in luminescent materials, the shortcomings of the traditional perovskites that limiting their practical applications, including the poor environmental, thermal, and optical stability, are being overcome gradually by controlling the composition between cations and halides or by replacing/doping cations at A- and B-sites with other metal cations, and so on [94]. Besides, more environmentally friendly lead-free halide perovskites make the practical application more likely [101].

The emerging carbon dots that can be easily prepared by green procedures have recently been demonstrated to be a superior color converter for realizing wLEDs excited by blue chips, which not only maintains the excellent luminescence performance of quantum dots, but also has the advantages of low toxicity, low cost and wide source of raw materials [102,103]. For instance, Shen et al. develop an in situ solvothermal process for synthesizing CDs using reaction mixture of urea, trisodium citrate and DMF, as shown in Fig. 7a [92]. The CDs show uniform distribution with an average particle diameter of 4.5 nm (Fig. 7b) and wLEDs devices with CCT of 4492 K can be achieved in the CDs based LEDs approaching to the coordinate (0.33, 0.33) of pure white light (Fig. 7c) [92]. In another work, a kind of CD powder with high PL QY of 65 % in the range of 500–620 nm was synthesized by a simple one-pot microwave heating method, and wLED with high luminous efficiencies (>90 $lm{\cdot}W^{-1}$) were realized using the CDs [93]. However, considering the high cost and difficulty to largely produce of these frontier luminescent materials, rare earth doped phosphor is still the main material to achieve wLEDs. Therefore, producing high-quality luminescent materials on a large scale remains challenging [104].

Although adding red phosphors has a more obvious effect on reducing the value of CCT compared to optimizing the existing yellow luminescent materials, the uneven grain size and specific gravity of phosphors make inhomogeneous color and intensity distribution in the whole system, which also reduces the conversion efficiency of phosphors. As a result, among these Optimization Strategies of tuning the emission spectrum of phosphors, optimizing the luminescent center ion or the structure of host of YAG:Ce is the simplest because this kind of phosphor with good performance can be obtained only by using cheap oxides as raw materials for high temperature calcination. While the high temperature and pressure environment required for the preparation of nitride phosphor requires higher performance of the equipment. Frontier luminescent materials with excellent performance, including semiconductor quantum dots, metal halide perovskites, and luminescent carbon dots, are prepared by colloidal and hydrothermal synthesis mainly, large-scale preparation of which is difficult and costly.

4.2. *Tuning the scattering processes of light*

In commercial wLEDs, the yellow-emitting phosphors were mixed with transparent encapsulating material and then dispersed in a cup reflector or directly coated on the LED chip surface. Due to the simplicity of preparation, the latter direct coating method can achieve mass production, but it suffers from propagation energy losses for the large difference of RI between semiconductor chips and encapsulating materials and it has been shown that nearly 60 % re-emitted yellow rays are backscattered to the LED chip, which seriously decreases the luminous flux [105]. In addition, this direct coating method results in poor quality in angular CCT and the unwanted phenomenon such as “yellow ring”. The scattering effect can strongly influence the optical path and weaken the CCT deviation in wLEDs. More importantly, it can increase the amount of received photons passing through layers of packages, which is crucial for the luminous efficiency of wLEDs [106]. There mainly are two methods to tuning the scattering of light, and adjusting structure of the wLEDs is an effective method to enhance the uniformity of CCT [27]. Besides, it has been discovered that scattering capability of nanoparticles not only enable better utilization of blue light which increased the luminous flux, but help to reduce angle-dependent CCT deviation in recent years [106–108].

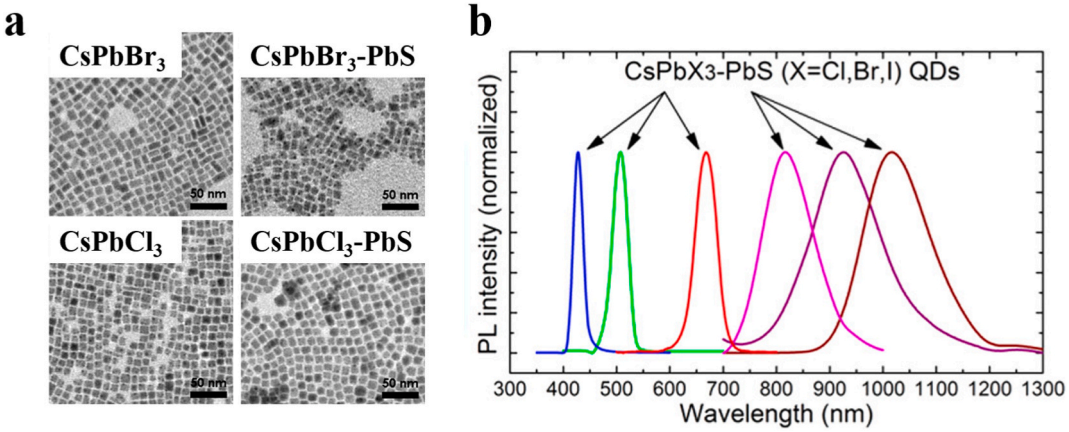

Fig. 6. a) TEM images and b) PL spectra of the $CsPbX_3$-PbS (Reprinted with permission from Ref. [98], copyright 2020, American Chemical Society).

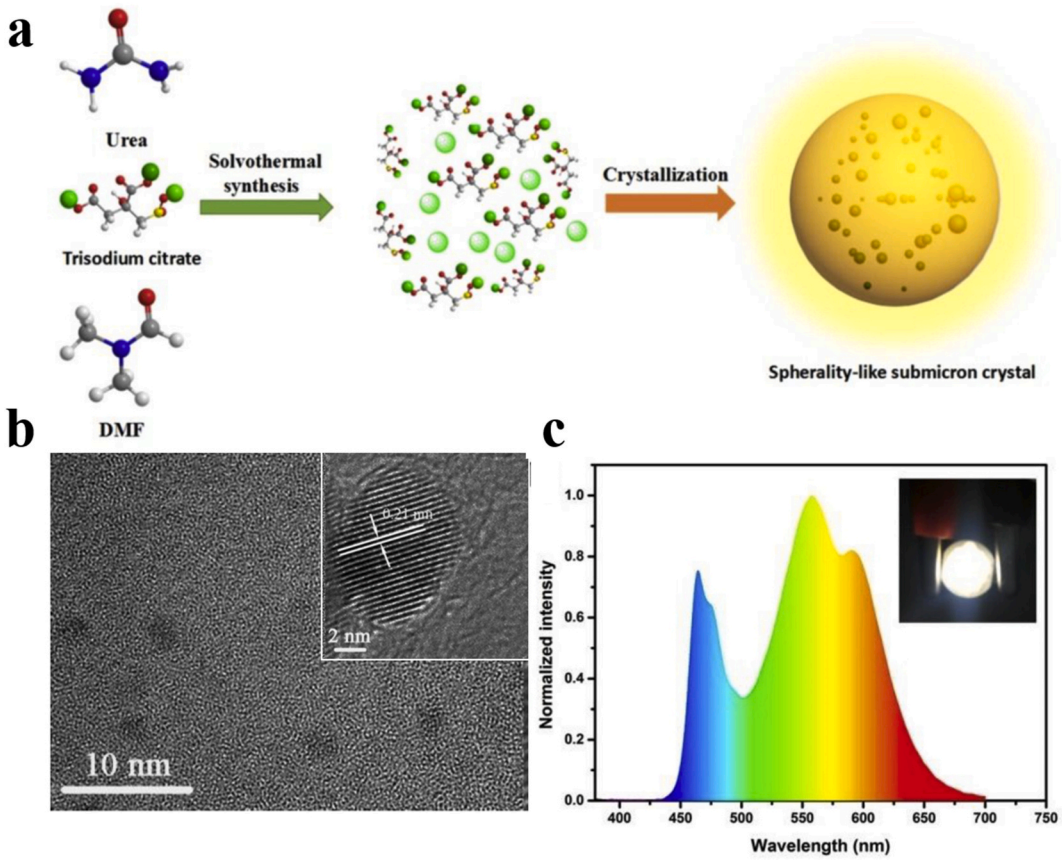

Fig. 7. a) Proposed in situ formation process of fluorescent CDs phosphors, b) TEM image of the NCDs in aqueous solution c) the emission spectrum of blue chip and LED based on CDs (Reprinted with permission from Ref. [92], copyright 2018, Elsevier). (For interpretation of the references to color in this figure legend, the reader is referred to the Web version of this article.)

4.2.1. Adjusting structure of the wLED

The remote phosphor coating method, separating the LED chip from the phosphor layer, can improve luminous efficacy by reducing the phosphor layer backscattering light reabsorbed by the blue LED chip [27,109]. Kuo et al. use Monte Carlo method to simulate both of conventional remote phosphor and patterned remote phosphor structures as shown in Fig. 8 [105]. Most of large angle of blue rays and backscattering yellow rays exit the package via the window region, ensuring the intensity ratio of yellow to blue rays with good constancy as compared to the conventional remote structure in larger divergent angle as shown in Fig. 8a and it can also concluded

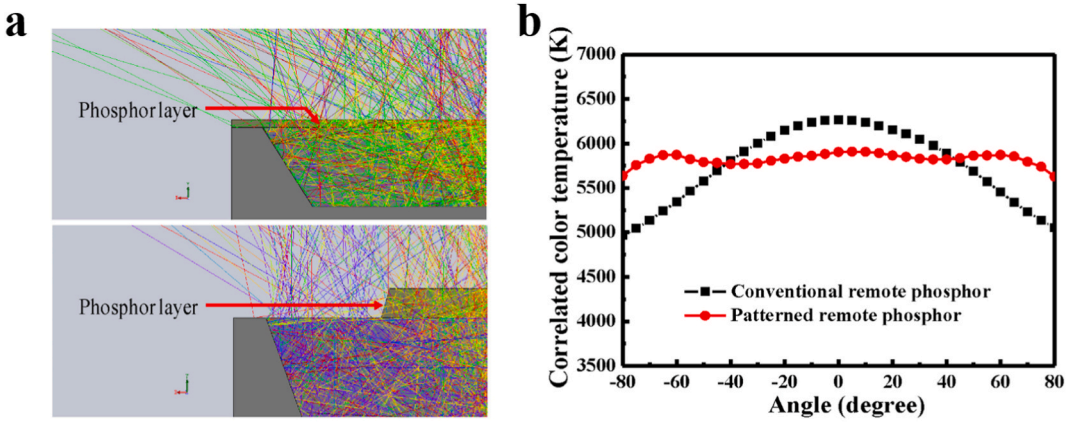

Fig. 8. a) The ray tracing simulation results, b) angular-dependent CCT(b) of two phosphor distribution structures (Reprinted with permission from Ref. [105], copyright 2011, Optical Society of America).

from the measurement data that the angular-dependent CCT of patterned remote phosphor structure was more uniform in larger angle distribution (Fig. 8b) [105]. For devices with textured sidewalls, the scattering probability of photons at the GaN/air interface is increased and the light extraction efficiency is enhanced since photons are allowed to find escape cones in the horizontal direction [110–112]. Compared with conventional LED without specific designs, LED with 45° sidewalls and a backside reflector can achieve significant improvement of 55.8 %, 49.3 %, 47.2 %, and 55.4 % in the light output power, luminous flux, external quantum efficiency, and wall-plug efficiency respectively [110]. Besides, LED with a hybrid structure incorporating a microhole array, 45° sidewalls, and an appropriate SiO_2 nanoparticle/microsphere passivation layer, shows 50.6 %, 50.9 %, 48.4 %, and 49.9 % enhancements in light output power, luminous flux, luminous efficacy, and wall-plug efficiency. The passivation layer play an important role in reducing reverse-biased leakage current, leading to substantial enhancements in optical properties while LED without any degradation in electrical performance [112]. In general, adjusting structure of the wLED can achieve a higher luminous flux and more uniform CCT by the increased scattering probability and opportunity to find photons escape cones.

4.2.2. Adding non-luminous nanoparticles to the encapsulant

Adding a certain amount of non-luminous nanoparticles to the encapsulant also can improve CCT uniformity and luminous flux of wLEDs, such as ZrO_2 [28,106,113], TiO_2 [114], cellulose nanocrystals (CNC) [107], as summarized in Table 4, since the use of scattering additive in the encapsulant can significantly influence the optical path. As the angular-dependent emission intensity, CNC-embedded wLED structures can exhibit superior performance and produce high-quality white light at different viewing angles. It was found that adding 6 wt% of CNCs to wLED increases the luminous flux by around 33 %, reduces the CCT from 4220 to 3985 K, and reduces angular-dependent CCT variation from 270 to 224 K [107]. Besides, scattering additive with high refractive index (RI) can improve the light extraction efficiency of LEDs because it can bridge the gap of RI between the chips through encapsulant to the air as shown in Fig. 9a and b [113]. Fig. 9a shows schematic diagram of LED encapsulation and the light extraction models at the interface, which indicating that the value of refractive index is one of the most important parameter while evaluating the performance of the encapsulation material to make devices with high light extraction efficiency [113]. Our group have developed a kind of wLED exhibiting significant enhanced luminous flux (form 13.28 to 31.34) and decreased proportion of blue light(3.1 %–1.3 %), resulting in low correlated color temperature was obtain by introducing ultrasmall ZrO_2 nanoparticles in commercial-grade silicone without any additional red phosphors (Fig. 9b) [28]. However, the commercial encapsulant are generally less compatible with nanoparticles leading to mass nanoparticles aggregate, which results in low transparency of light. Surface modification is an effective way to improve the dispersibility of particles [28,113,114]. As reported, the dispersibility of modified TiO_2 particles was greater than that of the as-prepared TiO_2 particles (1.6–2.5 times). Except that the luminous fluxes could be increased by 2.95%–11.79 % by adding TiO_2 particles in the encapsulant, which consistent with the above, the color uniformity will improve with the increasing dispersibility [114]. As a result, controlling the dispersion for nanoparticles in polymeric hosts to avoid the scattering of large aggregated particles and obtain optically transparent hybrid nanocomposites is crucial. Among these non-luminous nanoparticles, ZrO_2 exhibits a remarkable light scattering ability with high refractive (n: 2.18 at 500 nm) and without any visible light absorption due to its large bandgap energy, improving the CCT uniformity and luminous flux of wLEDs [115].

5. Conclusion and outlook

WLEDs has been widely used in daily lives and the property studies and preparation of the most commonly used phosphor YAG:Ce are nearly mature. Many scientists are devoted to exploring new materials or promoting the performance of existing luminescence materials to improve the performance of wLEDs toward energy-efficient, healthy and comfortable lighting. At present, a high CRI of more than 90 has been achieved by doping modification of YAG:Ce to make the original yellow phosphor emission wavelength redshift, and/or adding an appropriate amount of red phosphor into packaging materials. And the CCT uniformity and luminous flux are significantly improved by tuning the scattering of light, such as adjusting structure of the wLEDs, Adding a certain amount of non-luminous nanoparticles to the encapsulant. There are still the following points worth studying to optimize wLEDs: In view of tuning emission spectra, luminescent materials should be improved further, including a) improve the thermal stability of luminescent materials to ensure their stable performance in high power LED devices, b) enhance absorption of the material in the blue light region, that is, improve the light conversion efficiency of wLEDs pumped by blue chips, c) reduce the particle size of phosphors, which affect it's deposition in the packaging materials, to improve the light uniformity, d) optimize the phosphor production process, reduce energy consumption, and reduce the use of toxic raw materials, e) develop green preparation methods, expand the production scale of frontier luminescent materials, and reduce costs. On the other hand, it is also necessary to make full use of non-luminous particles for better utilization of blue light to increase the luminous flux, reducing angle-dependent CCT deviation. To solve the problem of transparency reducing caused by nanoparticles aggregation, the dispersion for nanoparticles in polymeric hosts should be controlled to avoid the scattering of large aggregated particles and obtain optically transparent hybrid nanocomposites.

Data availability statement

Data availability statement Data sharing is not applicable. No data was used for the research described in the article.

CRediT authorship contribution statement

Fen Wang: Writing – original draft, Conceptualization. **Hao Pan:** Writing – review & editing, Investigation, Conceptualization.

Table 4
Typical non-luminous nanoparticles tuning the scattering processes.

Nanoparticles	Luminous flux	CCT/K	CCT deviation/K	Reference
ZrO_2	31.34 (100 mA)	4573		[28]
ZrO_2	> 30 (120 mA)	< 4500	7	[106]
TiO_2	34.14 (121 mA)	7651.1	124.2	[114]
ZnO	70 (350 mA)		40	[108]
CNCs	328 (2.6 V)	< 4300	59	[107]

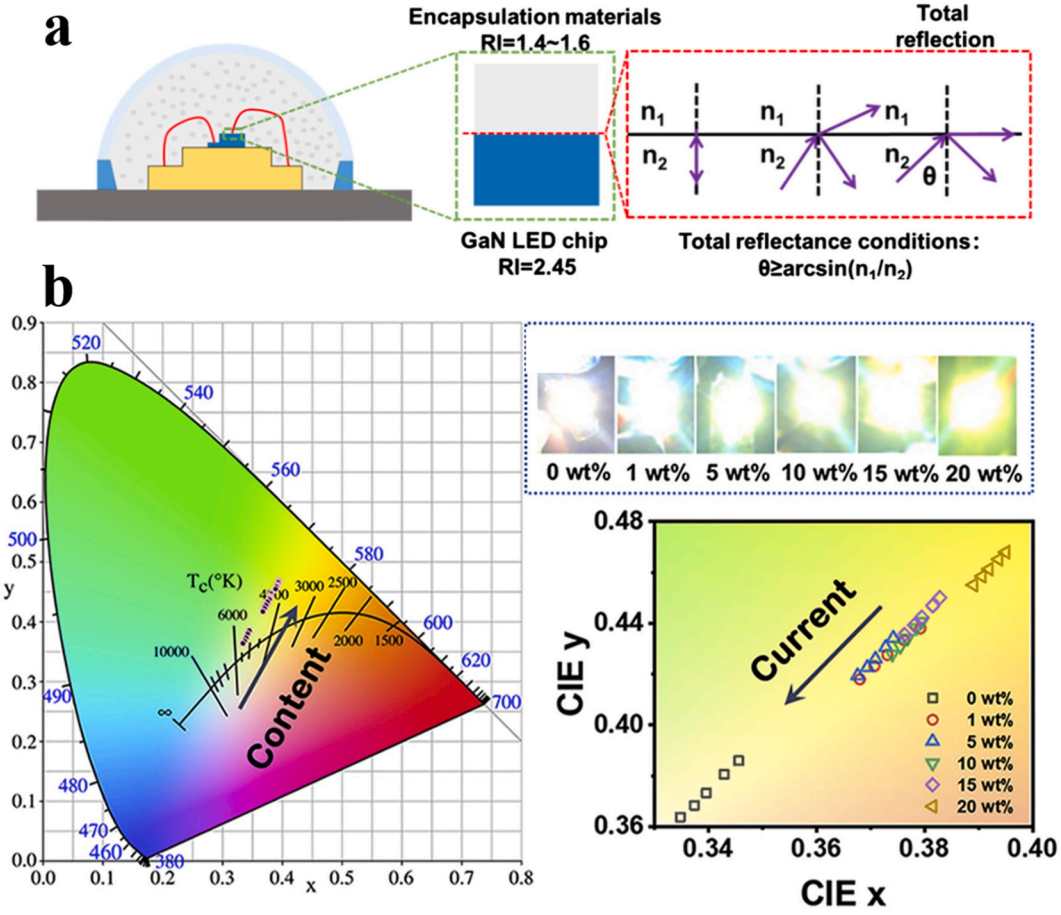

Fig. 9. a) schematic diagram of LED encapsulation and the light extraction models at the interface (Reprinted with permission from Ref. [113], copyright 2019, Elsevier), b) CIE color coordinates and optical photograph of the wLEDs (Reprinted with permission from Ref. [28], copyright 2019, Elsevier). (For interpretation of the references to color in this figure legend, the reader is referred to the Web version of this article.)

Wei Mao: Writing – review & editing, Resources. **Dan Wang:** Writing – review & editing, Supervision, Funding acquisition, Conceptualization.

Declaration of competing interest

The authors declare the following financial interests/personal relationships which may be considered as potential competing interests: Dan Wang is an associate editor of Heliyon Chemical Engineering Section. If there are other authors, they declare that they have no known competing financial interests or personal relationships that could have appeared to influence the work reported in this paper.

Acknowledgements

This work was supported by the National Natural Science Foundation of China (22278027) and Fundamental Research Funds for

the Central Universities of China (JD2403).

References

[1] A.C. Berends, M.A. van de Haar, M.R. Krames, YAG:Ce^{3+} phosphor: from micron-sized workhorse for general lighting to a bright future on the nanoscale, Chem. Rev. 120 (24) (2020) 13461–13479.
[2] M. Zhu, Y. Pan, L. Xi, H. Lian, J. Lin, Design, preparation, and optimized luminescence of a dodec-fluoride phosphor $Li_3Na_3A_{l2}F_{12}$:Mn^{4+} for warm WLED applications, J. Mater. Chem. C 5 (39) (2017) 10241–10250.
[3] T. Zhuang, Y. Lin, J. Jin, Z. Deng, Y. Peng, L. Gong, Z. Wang, K. Du, X. Huang, A mechanochemically synthesized hybrid bismuth halide as highly efficient red phosphor for blue chip-based wLED, Adv. Opt. Mater. 11 (12) (2023) 2202951.
[4] A. Katsnelson, Lighting design for better health and well being, Nature 568 (7751) (2019).
[5] P.M. Pattison, J.Y. Tsao, G.C. Brainard, B. Bugbee, LEDs for photons, physiology and food, Nature 563 (7732) (2018) 493–500.
[6] K.J. Gaston, Lighting up the nighttime, Science 362 (6416) (2018) 744–746.
[7] K. Zielinska-Dabkowska, Make lighting healthier, Nature 553 (7688) (2018) 274–276.
[8] L.-F. Hung, B. Arumugam, Z. She, L. Ostrin, E.L. Smith, Narrow-band, long-wavelength lighting promotes hyperopia and retards vision-induced myopia in infant rhesus monkeys, Exp. Eye Res. 176 (2018) 147–160.
[9] L. Tian, K. Cao, D.-L. Ma, S.-Q. Zhao, L.-X. Lu, A. Li, C.-X. Chen, C.-R. Ma, Z.-F. Ma, Y. Jie, Investigation of the efficacy and safety of 650 nm low-level red light for myopia control in children: a randomized controlled trial, Ophthalmology and Therapy 11 (6) (2022) 2259–2270.
[10] G. Liu, B. Li, H. Rong, B. Du, B. Wang, J. Hu, B. Zhang, R. Wei, Axial length shortening and choroid thickening in myopic adults treated with repeated low-level red light, J. Clin. Med. 11 (24) (2022) 7498.
[11] F. Behar-Cohen, C. Martinsons, F. Viénot, G. Zissis, A. Barlier-Salsi, J.P. Cesarini, O. Enouf, M. Garcia, S. Picaud, D. Attia, Light-emitting diodes (LED) for domestic lighting: any risks for the eye? Prog. Retin. Eye Res. 30 (4) (2011) 239–257.
[12] X. Li, S. Zhu, F. Qi, Blue light pollution causes retinal damage and degeneration by inducing ferroptosis, J. Photochem. Photobiol. B Biol. 238 (2023) 112617.
[13] I. Jaadane, G. Villalpando Rodriguez, P. Boulenguez, S. Carré, I. Dassieni, C. Lebon, S. Chahory, F. Behar-Cohen, C. Martinsons, A. Torriglia, Retinal phototoxicity and the evaluation of the blue light hazard of a new solid-state lighting technology, Sci. Rep. 10 (1) (2020) 6733.
[14] Z. She, L.-F. Hung, B. Arumugam, K.M. Beach, E.L. Smith Iii, The effects of reduced ambient lighting on lens compensation in infant rhesus monkeys, Vis. Res. 187 (2021) 14–26.
[15] J. Cai, W. Hao, Y. Li, S. Zeng, Y. Guo, S. Tang, R. Wen, L. Pan, J. Fan, P. Tang, A better photometric index of photo-biological effect on visual function of human eye: illuminance or luminance? IEEE Access 7 (2019) 165919–165927.
[16] Y. Fang, C. Liu, C. Zhao, H. Zhang, W. Wang, N. Zou, A study of the effects of different indoor lighting environments on computer work fatigue, Int. J. Environ. Res. Publ. Health 19 (11) (2022) 6866.
[17] H. Rolf, L. Udovicic, S. Völker, Light exposure in home-based work: can a simple lighting system increase alertness? Light. Res. Technol. (2023) 14771535231158029.
[18] W. Schobersberger, C. Blank, F. Hanser, A. Griesmacher, M. Canazei, V. Leichtfried, Impact of a single, short morning bright light exposure on tryptophan pathways and visuo- and sensorimotor performance: a crossover study, J. Physiol. Anthropol. 37 (1) (2018) 12.
[19] T. Ru, Y.A.W. de Kort, K.C.H.J. Smolders, Q. Chen, G. Zhou, Non-image forming effects of illuminance and correlated color temperature of office light on alertness, mood, and performance across cognitive domains, Build. Environ. 149 (2019) 253–263.
[20] D.C. Fernandez, P.M. Fogerson, L. Lazzerini Ospri, M.B. Thomsen, R.M. Layne, D. Severin, J. Zhan, J.H. Singer, A. Kirkwood, H. Zhao, D.M. Berson, S. Hattar, Light affects mood and learning through distinct retina-brain pathways, Cell 175 (1) (2018) 71–84.e18.
[21] Y. Wang, T. Deboer, Hypnotic effects of melatonin depend on the environmental lighting conditions in the rat, J. Pineal Res. (2023) e12928.
[22] H. Tian, T. Chen, Y. Hu, T. Guan, M. Cai, Change of circadian effect with colour temperature and eye spectral transmittance at different ages, Light. Res. Technol. 53 (1) (2021) 41–53.
[23] T. Weil, K.M. Daly, H. Yarur Castillo, M.B. Thomsen, H. Wang, M.E. Mercau, S. Hattar, H. Tejeda, D.C. Fernandez, Daily changes in light influence mood via inhibitory networks within the thalamic perihabenular nucleus, Sci. Adv. 8 (23) (2022) eabn3567.
[24] Y. Zeng, H. Sun, J. Yu, B. Lin, Effects of correlated color temperature of office light on subjective perception, mood and task performance, Build. Environ. 224 (2022) 109508.
[25] Y. Li, F. Shen, L. Hu, Z. Lang, Q. Liu, F. Cai, L. Fu, A stare-down video-rate high-throughput hyperspectral imaging system and its applications in biological sample sensing, IEEE Sensor. J. 23 (19) (2023) 23629–23637.
[26] P. Zhu, H. Zhu, G.C. Adhikari, S. Thapa, Design of circadian white light-emitting diodes with tunable color temperature and nearly perfect color rendition, OSA Continuum 2 (8) (2019) 2413–2427.
[27] H.-T. Lin, C.-H. Tien, C.-P. Hsu, R.-H. Horng, White thin-film flip-chip LEDs with uniform color temperature using laser lift-off and conformal phosphor coating technologies, Opt Express 22 (26) (2014) 31646–31653.
[28] X. He, R. Tang, Y. Pu, J.-X. Wang, Z. Wang, D. Wang, J.-F. Chen, High-gravity-hydrolysis approach to transparent nanozirconia/silicone encapsulation materials of light emitting diodes devices for healthy lighting, Nano Energy 62 (2019) 1–10.
[29] X. Zhang, H. Yang, Z. Wan, T. Su, X. Zhang, J. Zhuang, B. Lei, Y. Liu, C. Hu, Self-quenching-resistant red emissive carbon dots with high stability for warm white light-emitting diodes with a high color rendering index, Adv. Opt. Mater. 8 (15) (2020) 2000251.
[30] B. Xie, H. Liu, R. Hu, C. Wang, J. Hao, K. Wang, X. Luo, Targeting cooling for quantum dots in white QDs-LEDs by hexagonal boron nitride platelets with electrostatic bonding, Adv. Funct. Mater. 28 (30) (2018) 1801407.
[31] Y. Tang, X. He, Y. Zhang, H. Yuan, Y. Xin, X. Ren, Q. Chen, H. Yin, Anchoring of red perovskite nanocrystals on YAG:Ce phosphor for high color rendering index WLEDs, J. Alloys Compd. 899 (2022) 163347.
[32] Z. Hou, X. Tang, X. Luo, T. Zhou, L. Zhang, R.-J. Xie, A green synthetic route to the highly efficient K_2SiF_6:Mn^{4+} narrow-band red phosphor for warm white light-emitting diodes, J. Mater. Chem. C 6 (11) (2018) 2741–2746.
[33] Z. Wang, F. Yuan, X. Li, Y. Li, H. Zhong, L. Fan, S. Yang, 53% efficient red emissive carbon quantum dots for high color rendering and stable warm white-light-emitting diodes, Adv. Mater. 29 (37) (2017) 1702910.
[34] Z. Leng, H. Bai, Q. Qing, H. He, J. Hou, B. Li, Z. Tang, F. Song, H. Wu, A zero-thermal-quenching blue phosphor for sustainable and human-centric wLED lighting, ACS Sustain. Chem. Eng. 10 (33) (2022) 10966–10977.
[35] T. Yuan, F. Yuan, X. Li, Y. Li, L. Fan, S. Yang, Fluorescence–phosphorescence dual emissive carbon nitride quantum dots show 25% white emission efficiency enabling single-component WLEDs, Chem. Sci. 10 (42) (2019) 9801–9806.
[36] R. Su, D. Wang, M. Liu, J. Yan, J.-X. Wang, Q. Zhan, Y. Pu, N.R. Foster, J.-F. Chen, Subgram-scale synthesis of biomass waste-derived fluorescent carbon dots in subcritical water for bioimaging, sensing, and solid-state patterning, ACS Omega 3 (10) (2018) 13211–13218.
[37] G. Hu, Y. Wang, S. Zhang, H. Ding, Z. Zhou, J. Wei, X. Li, H. Xiong, Rational synthesis of silane-functionalized carbon dots with high-efficiency full-color solid-state fluorescence for light emitting diodes, Carbon 203 (2023) 1–10.
[38] Z. Yan, T. Chen, L. Yan, X. Liu, J. Zheng, F.-d. Ren, Y. Yang, B. Liu, X. Liu, B. Xu, One-step synthesis of white-light-emitting carbon dots for white LEDs with a high color rendering index of 97, Adv. Sci. 10 (12) (2023) 2206386.
[39] X. Wang, B. Wang, H. Wang, T. Zhang, H. Qi, Z. Wu, Y. Ma, H. Huang, M. Shao, Y. Liu, Y. Li, Z. Kang, Carbon-dot-based white-light-emitting diodes with adjustable correlated color temperature guided by machine learning, Angew. Chem. Int. Ed. 60 (22) (2021) 12585–12590.
[40] Z. Wang, N. Jiang, M. Liu, R. Zhang, F. Huang, D. Chen, Bright electroluminescent white-light-emitting diodes based on carbon dots with tunable correlated color temperature enabled by aggregation, Small 17 (52) (2021) 2104551.

[41] R. Valleix, Q. Zhang, D. Boyer, P. Boutinaud, G. Chadeyron, Y. Feng, H. Okuno, F. Réveret, H. Hintze-Bruening, F. Leroux, A first wide-open LDH structure hosting InP/ZnS QDs: a new route toward efficient and photostable red-emitting phosphor, Adv. Mater. 33 (38) (2021) 2103411.

[42] C. Li, X.-M. Wang, Z.-P. Yang, H. Jiao, $Ca_8Mg_7Si_9N_{22}:Ce^{3+}$—a yellow-emitting nitride phosphor for white light emitting diodes, ACS Appl. Electron. Mater. 2 (4) (2020) 936–943.

[43] Y.-Y. Zhou, E.-H. Song, T.-T. Deng, Q.-Y. Zhang, Waterproof narrow-band fluoride red phosphor $K_2TiF_6:Mn^{4+}$ via facile superhydrophobic surface modification, ACS Appl. Mater. Interfaces 10 (1) (2018) 880–889.

[44] L. Feng, S. Pi, J. Zheng, W. Liang, J. Li, T. Zhou, M. Liu, Y. Zhao, X. Lai, J. Bi, D. Gao, Realizing thermal and moisture stability in the $K_2Ge_{1-x}Ti_xF_6:Mn^{4+}$ red phosphors with high efficiency for WLEDs, Ceram. Int. 49 (16) (2023) 27486–27495.

[45] Q. Zhang, J. Li, W. Jiang, L. Lin, J. Ding, M.G. Brik, M.S. Molokeev, H. Ni, M. Wu, $CaY_2Al_4SiO_{12}:Ce^{3+},Mn^{2+}$: a single component phosphor to produce high color rendering index WLEDs with a blue chip, J. Mater. Chem. C 9 (34) (2021) 11292–11298.

[46] J. Zhou, Y. Chen, C. Jiang, B. Milićević, M.S. Molokeev, M.G. Brik, I.A. Bobrikov, J. Yan, J. Li, M. Wu, High moisture resistance of an efficient Mn^{4+}-activated red phosphor $Cs_2NbOF_5:Mn^{4+}$ for WLEDs, Chem. Eng. J. 405 (2021) 126678.

[47] Y. Zhou, S. Zhang, X. Wang, H. Jiao, Structure and luminescence properties of Mn^{4+}-activated $K_3TaO_2F_4$ red phosphor for white LEDs, Inorg. Chem. 58 (7) (2019) 4412–4419.

[48] X. Zhang, Y.-T. Tsai, S.-M. Wu, Y.-C. Lin, J.-F. Lee, H.-S. Sheu, B.-M. Cheng, R.-S. Liu, Facile atmospheric pressure synthesis of high thermal stability and narrow-band red-emitting $SrLiAl_3N_4:Eu^{2+}$ phosphor for high color rendering index white light-emitting diodes, ACS Appl. Mater. Interfaces 8 (30) (2016) 19612–19617.

[49] H. Li, Q. Wu, Z. An, J. Ding, A broadband yellow-emitting nitridoalumosilicate $Ca_4SiAl_3N_7:Ce^{3+}$ phosphor for solid-state lighting, Ceram. Int. 49 (8) (2023) 12491–12498.

[50] Y. Tian, Y. Tang, X. Yi, G. Ao, J. Chen, D. Hao, Y. Lin, S. Zhou, The analyses of structure and luminescence in $(Mg_yY_{3-y})(Al_{5-y}Si_y)O_{12}$ and $Y_3(Mg_xAl_{5-2x}Si_x)O_{12}$ ceramic phosphors, J. Alloys Compd. 813 (2020) 152236.

[51] A. Sánchez de Miguel, J. Bennie, E. Rosenfeld, S. Dzurjak, K.J. Gaston, Environmental risks from artificial nighttime lighting widespread and increasing across Europe, Sci. Adv. 8 (37) (2022) eabl6891.

[52] D.Y. Kosyanov, X. Liu, A.A. Vornovskikh, A.A. Kosianova, A.M. Zakharenko, A.P. Zavjalov, O.O. Shichalin, V.Y. Mayorov, V.G. Kuryavyi, X. Qian, J. Zou, J. Li, Al_2O_3–Ce:YAG and Al_2O_3–Ce:(Y,Gd)AG composite ceramics for high brightness lighting: effect of microstructure, Mater. Char. 172 (2021) 110883.

[53] S. Arjoca, D. Inomata, Y. Matsushita, K. Shimamura, Growth and optical properties of $(Y_{1-x}Gd_x)_3Al_5O_{12}$:Ce single crystal phosphors for high-brightness neutral white LEDs and LDs, CrystEngComm 18 (25) (2016) 4799–4806.

[54] Y. Duan, C. Zhao, H. Lin, R. Hong, C. Tao, Z. Han, D. Zhang, S. Zhou, Photoluminescence properties of $Tb_3Al_5O_{12}:Ce^{3+}$, Mn^{2+} phosphor ceramics for high color rendering index warm white LEDs, Opt. Mater. 111 (2021) 110670.

[55] A. Markovskyi, V. Gorbenko, T. Zorenko, S. Witkiewicz-Lukaszek, O. Sidletskiy, A. Fedorov, Y. Zorenko, Development of three-layered composite color converters for white LEDs based on the epitaxial structures of YAG:Ce, TbAG:Ce and LuAG:Ce garnets, Materials 16 (5) (2023) 1848.

[56] W.T. Hong, J.H. Lee, J.W. Son, Z. Lee, H.J. Park, H.S. Kim, J.S. Lee, H.K. Yang, Color rendering improvement of the YAG:Ce^{3+} phosphors by co-doping with Gd^{3+} ions, Ceram. Int. 42 (2, Part A) (2016) 2204–2208.

[57] F. Wang, M. Wang, Y. Liu, Y. Pu, J.-X. Wang, D. Wang, J.-F. Chen, Intensified synthetic approach for GdYAG:Ce phosphors with ultrahigh color rendering toward healthy lighting, AIChE J. 70 (1) (2024) e18253.

[58] M. Shang, J. Fan, H. Lian, Y. Zhang, D. Geng, J. Lin, A double substitution of Mg^{2+}–Si^{4+}/Ge^{4+} for $Al(1)^{3+}$–$Al(2)^{3+}$ in Ce^{3+}-doped garnet phosphor for white LEDs, Inorg. Chem. 53 (14) (2014) 7748–7755.

[59] Q. Du, S. Feng, H. Qin, H. Hua, H. Ding, L. Jia, Z. Zhang, J. Jiang, H. Jiang, Massive red-shifting of Ce^{3+} emission by Mg^{2+} and Si^{4+} doping of YAG:Ce transparent ceramic phosphors, J. Mater. Chem. C 6 (45) (2018) 12200–12205.

[60] J. Jia, Y. Qiang, J. Xu, M. Liang, W. Wang, F. Yang, J. Cui, Q. Dong, X. Ye, A comparison study on the substitution of Y^{3+}–Al^{3+} by M^{2+}–Si^{4+}(M = Ba, Sr, Ca, Mg) in $Y_3Al_5O_{12}$: Ce^{3+} phosphor, J. Am. Ceram. Soc. 103 (9) (2020) 5111–5119.

[61] Y. Zheng, W. Zhuang, X. Xing, R. Liu, Y. Li, Y. Liu, Y. Hu, X. Chen, L. Chen, X. Ma, Carbon interstitial defects causing emission red shift in YAG:Ce phosphor: first-principles calculation, J. Rare Earths 36 (12) (2018) 1239–1244.

[62] G. Ao, Y. Tang, X. Yi, Y. Tian, J. Chen, D. Hao, Y. Lin, S. Zhou, Red emission generation in Ce^{3+}/Mn^{2+} co-doping $Y_3Al_5O_{12}$ phosphor ceramics for warm white lighting emitting diodes, J. Alloys Compd. 798 (2019) 695–699.

[63] J. Ling, Y. Zhou, W. Xu, H. Lin, S. Lu, B. Wang, K. Wang, Red-emitting YAG: Ce, Mn transparent ceramics for warm WLEDs application, Journal of Advanced Ceramics 9 (1) (2020) 45–54.

[64] Y. Tang, S. Zhou, X. Yi, D. Hao, X. Shao, J. Chen, The characterization of Ce/Pr-doped YAG phosphor ceramic for the white LEDs, J. Alloys Compd. 745 (2018) 84–89.

[65] Y. Li, Y. Liu, Z. Luo, Z. Liu, S. Hanson, C. Pang, H. Lin, H. Qin, J. Jiang, Ce/Mn/Cr: $Y_3Al_5O_{12}$ phosphor ceramics for white LED and LD lighting with a high color rendering index, Ceram. Int. 49 (15) (2023) 24703–24711.

[66] C. He, T. Takeda, Z. Huang, J. Xu, J. Chen, W. Yi, R. Xie, N. Hirosaki, Powder synthesis and luminescence of a novel yellow-emitting $Ba_5Si_{11}Al_7N_{25}$: Eu^{2+} phosphor discovered by a single-particle-diagnosis approach for warm w-LEDs, Chem. Eng. J. 455 (2023) 140932.

[67] T. Suehiro, N. Hirosaki, R.-J. Xie, Synthesis and photoluminescent properties of $(La,Ca)_3Si_6N_{11}:Ce^{3+}$ fine powder phosphors for solid-state lighting, ACS Appl. Mater. Interfaces 3 (3) (2011) 811–816.

[68] J. Ding, H. You, Y. Wang, B. Ma, X. Zhou, X. Ding, Y. Cao, H. Chen, W. Geng, Y. Wang, Site occupation and energy transfer of Ce^{3+}-activated lithium nitridosilicate $Li_2SrSi_2N_4$ with broad-yellow-light-emitting property and excellent thermal stability, J. Mater. Chem. C 6 (13) (2018) 3435–3444.

[69] Z. Xia, A. Meijerink, Ce^{3+}-Doped garnet phosphors: composition modification, luminescence properties and applications, Chem. Soc. Rev. 46 (1) (2017) 275–299.

[70] C. Shao, L. Zhang, T. Zhou, P. Gao, J. Kang, B. Sun, C. Hou, Y. Li, Q. Yao, J. Wu, H. Chen, Tunable blue/yellow emission in high-power white LED devices packaged with Ce:(Y, Gd)AG transparent ceramics, Ceram. Int. 45 (11) (2019) 14420–14425.

[71] P. Huang, Y. Zhao, J. Wang, Y. Zheng, P. Yang, Q. Zheng, S. Gu, B. Zhou, W. Jiang, L. Wang, Tunable chromaticity and high color rendering index of WLEDs with $CaAlSiN_3:Eu^{2+}$ and YAG:Ce^{3+} dual phosphor-in-silica-glass, J. Am. Ceram. Soc. 103 (9) (2020) 4989–4998.

[72] L. Yang, N. Zhang, R. Zhang, B. Wen, H. Li, X. Bian, A CaS:Eu based red-emitting phosphor with significantly improved thermal quenching resistance for LED lighting applications, Mater. Lett. 129 (2014) 134–136.

[73] C. Zhang, T. Uchikoshi, R.-J. Xie, L. Liu, Y. Cho, Y. Sakka, N. Hirosaki, T. Sekiguchi, Reduced thermal degradation of the red-emitting $Sr_2Si_5N_8:Eu^{2+}$ phosphor via thermal treatment in nitrogen, J. Mater. Chem. C 3 (29) (2015) 7642–7651.

[74] J. Ding, Q. Wu, Y. Li, Q. Long, Y. Wang, Y. Wang, Eu^{2+}-activated $Ca_5Si_2Al_2N_8$ – a novel nitridoalumosilicate red phosphor containing the special polyhedron of separated corner-shared $[Al_2N_6]$ and $[Si_2N_6]$, Chem. Eng. J. 302 (2016) 466–474.

[75] J. Wang, L. Dong, Z. Lyu, D. Sun, T. Tan, H. You, Facile synthesis of highly efficient and thermally stable $BaAl_4Sb_2O_{12}:Eu^{2+}$ phosphor in air, Adv. Funct. Mater. 33 (20) (2023) 2214611.

[76] Y. Liu, R. Zhang, K. Yan, J.-F. Sun, Ultrahighly efficient narrowband red luminescence of uniquely distorted Mn^{4+} octahedron in the feldspar-type LED phosphor, Laser Photon. Rev. 17 (8) (2023) 2200940.

[77] F. Liu, Y. Chen, B. Milićević, C. Jiang, S. Huang, L. Zhou, J. Zhou, M. Wu, Hydroquinone-modified Mn^{4+}-activated fluoride red phosphors with improved water-resistance, Colloids Surf. A Physicochem. Eng. Asp. 661 (2023) 130954.

[78] L. Huang, Y. Zhu, X. Zhang, R. Zou, F. Pan, J. Wang, M. Wu, HF-free hydrothermal route for synthesis of highly efficient narrow-band red emitting phosphor $K_2Si_{1-x}F_6:xMn^{4+}$ for warm white light-emitting diodes, Chem. Mater. 28 (5) (2016) 1495–1502.

[79] F. Hong, G. Pang, L. Diao, Z. Fu, G. Liu, X. Dong, W. Yu, J. Wang, Local structure modulation of Mn^{4+}-doped $Na_2Si_{1-y}Ge_yF_6$ red phosphors for enhancement of emission intensity, moisture resistance, thermal stability and application in warm pc-WLEDs, Dalton Trans. 49 (39) (2020) 13805–13817.

[80] S. Gu, M. Xia, C. Zhou, Z. Kong, M.S. Molokeev, L. Liu, W.-Y. Wong, Z. Zhou, Red shift properties, crystal field theory and nephelauxetic effect on Mn^{4+}-doped $SrMgAl_{10-y}Ga_yO_{17}$ red phosphor for plant growth LED light, Chem. Eng. J. 396 (2020) 125208.

[81] Q. Wang, J. Liao, L. Kong, B. Qiu, J. Li, H. Huang, H.-r. Wen, Luminescence properties of a non-rare-earth doped oxyfluoride $LiAl_4O_6F:Mn^{4+}$ red phosphor for solid-state lighting, J. Alloys Compd. 772 (2019) 499–506.

[82] T.T. Deng, E.H. Song, J. Sun, L.Y. Wang, Y. Deng, S. Ye, J. Wang, Q.Y. Zhang, The design and preparation of the thermally stable, Mn^{4+} ion activated, narrow band, red emitting fluoride $Na_3GaF_6:Mn^{4+}$ for warm WLED applications, J. Mater. Chem. C 5 (11) (2017) 2910–2918.

[83] Y. Zhu, L. Huang, R. Zou, J. Zhang, J. Yu, M. Wu, J. Wang, Q. Su, Hydrothermal synthesis, morphology and photoluminescent properties of an Mn^{4+}-doped novel red fluoride phosphor elpasolite K_2LiAlF_6, J. Mater. Chem. C 4 (24) (2016) 5690–5695.

[84] S. Wang, T. Seto, B. Liu, Y. Wang, C. Li, Z. Liu, H. Dong, Tremendous acceleration of plant growth by applying a new sunlight converter $Sr_4Al_{14-x}Ga_xO_{25}:Mn^{4+}$ breaking parity forbidden transition, Adv. Sci. 10 (2) (2023) 2204418.

[85] Y. Jin, Y. Hu, H. Wu, H. Duan, L. Chen, Y. Fu, G. Ju, Z. Mu, M. He, A deep red phosphor $Li_2MgTiO_4:Mn^{4+}$ exhibiting abnormal emission: potential application as color converter for warm w-LEDs, Chem. Eng. J. 288 (2016) 596–607.

[86] W.-W. Hu, C. Cai, Q.-Q. Zhu, X. Xu, L.-Y. Hao, S. Agathopoulos, Preparation of high performance $CaAlSiN_3:Eu^{2+}$ phosphors with the aid of BaF2 flux, J. Alloys Compd. 613 (2014) 226–231.

[87] W. Wu, Z. Zhang, R. Dong, G. Xie, J. Zhou, K. Wu, H. Zhang, Q. Cai, B. Lei, Characterization and properties of a $Sr_2Si_5N_8:Eu^{2+}$-based light-conversion agricultural film, J. Rare Earths 38 (5) (2020) 539–545.

[88] X. Zhang, Z. Dong, J. Shi, M. Gong, Luminescence properties of color-tunable zinc-codoped alikali earth sulfide phosphor for LED application, Mater. Lett. 76 (2012) 113–116.

[89] Y. Hu, W. Zhuang, H. Ye, S. Zhang, Y. Fang, X. Huang, Preparation and luminescent properties of $(Ca_{1-x},Sr_x)S:Eu^{2+}$ red-emitting phosphor for white LED, J. Lumin. 111 (3) (2005) 139–145.

[90] W. Yang, P. Zhong, S. Mei, Q. Chen, W. Zhang, J. Zhu, R. Guo, G. He, Photometric optimization of color temperature tunable quantum dots converted white LEDs for excellent color rendition, IEEE Photon. J. 8 (5) (2016) 1–11.

[91] D. Su, L. Wang, M. Li, S. Mei, X. Wei, H. Dai, Z. Hu, F. Xie, R. Guo, Highly luminescent water-soluble $AgInS_2/ZnS$ quantum dots-hydrogel composites for warm white LEDs, J. Alloys Compd. 824 (2020) 153896.

[92] C.-L. Shen, J.-H. Zang, Q. Lou, L.-X. Su, Z. Li, Z.-Y. Liu, L. Dong, C.-X. Shan, In-situ embedding of carbon dots in a trisodium citrate crystal matrix for tunable solid-state fluorescence, Carbon 136 (2018) 359–368.

[93] Y. Zhang, P. Zhuo, H. Yin, Y. Fan, J. Zhang, X. Liu, Z. Chen, Solid-state fluorescent carbon dots with aggregation-induced yellow emission for white light-emitting diodes with high luminous efficiencies, ACS Appl. Mater. Interfaces 11 (27) (2019) 24395–24403.

[94] H. Lu, Y. Sun, M. Li, Q. Wang, R. Wang, P. Zhu, G. Wang, $CsPbBr_3$:Na with an adjustable bandgap, improved luminescence stability, and its application in wLEDs with excellent color quality and vision performance, Adv. Funct. Mater. 33 (10) (2023) 2212767.

[95] Y. Zhang, J. Mao, P. Zhu, G. Wang, Tunable multicolor luminescence in vanadates from yttrium to indium with enhanced luminous efficiency and stability for its application in wLEDs and indoor photovoltaics, Nano Res. 16 (8) (2023) 11486–11494.

[96] J. Mao, D. Venugopal, Y. Zhang, P. Zhu, G. Wang, Synthesis and DFT calculation of germanium halide perovskites with high luminescent stability, and their applications in wLEDs and indoor photovoltaics, Chem. Eng. J. 470 (2023) 144160.

[97] W. Zhang, S. Ding, W. Zhuang, D. Wu, P. Liu, X. Qu, H. Liu, H. Yang, Z. Wu, K. Wang, X.W. Sun, InP/ZnS/ZnS core/shell blue quantum dots for efficient light-emitting diodes, Adv. Funct. Mater. 30 (49) (2020) 2005303.

[98] X. Zhang, X. Wu, X. Liu, G. Chen, Y. Wang, J. Bao, X. Xu, X. Liu, Q. Zhang, K. Yu, W. Wei, J. Liu, J. Xu, H. Jiang, P. Wang, X. Wang, Heterostructural $CsPbX_3$-PbS (X = Cl, Br, I) quantum dots with tunable Vis–NIR Dual emission, J. Am. Chem. Soc. 142 (9) (2020) 4464–4471.

[99] P. Zhu, H. Zhu, G.C. Adhikari, S. Thapa, Spectral optimization of white light from hybrid metal halide perovskites, OSA Continuum 2 (6) (2019) 1880–1888.

[100] P. Zhu, S. Thapa, H. Zhu, D. Venugopal, A. Sambou, Y. Yue, S.S. Dantuluri, S. Gangopadhyay, solid-state white light-emitting diodes based on 3D-Printed $CsPbX_3$-resin color conversion layers, ACS Appl. Electron. Mater. 5 (10) (2023) 5316–5324.

[101] P. Zhu, S. Thapa, H. Zhu, S. Wheat, Y. Yue, D. Venugopal, Composition engineering of lead-free double perovskites towards efficient warm white light emission for health and well-being, J. Alloys Compd. 960 (2023) 170836.

[102] S. Fan, X. Zheng, Q. Zhan, H. Zhang, H. Shao, J. Wang, C. Cao, M. Zhu, D. Wang, Y. Zhang, Super-strong and intrinsically fluorescent silkworm silk from carbon nanodots feeding, Nano-Micro Lett. 11 (1) (2019) 75.

[103] C. Tan, C. Zhou, X. Peng, H. Zhi, D. Wang, Q. Zhan, S. He, Sulfuric acid assisted preparation of red-emitting carbonized polymer dots and the application of bio-imaging, Nanoscale Res. Lett. 13 (1) (2018) 272.

[104] J. Leng, J. Chen, D. Wang, J.-X. Wang, Y. Pu, J.-F. Chen, Scalable preparation of $Gd_2O_3:Yb^{3+}/Er^{3+}$ upconversion nanophosphors in a high-gravity rotating packed bed reactor for transparent upconversion luminescent films, Ind. Eng. Chem. Res. 56 (28) (2017) 7977–7983.

[105] H.-C. Kuo, C.-W. Hung, H.-C. Chen, K.-J. Chen, C.-H. Wang, C.-W. Sher, C.-C. Yeh, C.-C. Lin, C.-H. Chen, Y.-J. Cheng, Patterned structure of remote phosphor for phosphor-converted white LEDs, Opt Express 19 (S4) (2011) A930–A936.

[106] K.-J. Chen, H.-V. Han, H.-C. Chen, C.-C. Lin, S.-H. Chien, C.-C. Huang, T.-M. Chen, M.-H. Shih, H.-C. Kuo, White light emitting diodes with enhanced CCT uniformity and luminous flux using ZrO_2 nanoparticles, Nanoscale 6 (10) (2014) 5378–5383.

[107] F.I. Chowdhury, Q. Xu, X. Wang, Improving the light quality of white light-emitting diodes using cellulose nanocrystal-filled phosphors, Advanced Photonics Research 2 (5) (2021) 2100006.

[108] L. Rao, Y. Tang, Z. Li, X. Ding, J. Li, S. Yu, C. Yan, H. Lu, Effect of ZnO nanostructures on the optical properties of white light-emitting diodes, Opt Express 25 (8) (2017) A432–A443.

[109] P. Acuña, S. Leyre, J. Audenaert, Y. Meuret, G. Deconinck, P. Hanselaer, Power and photon budget of a remote phosphor LED module, Opt Express 22 (S4) (2014) A1079–A1092.

[110] C.Y. Chen, W.C. Liu, Light extraction enhancement of GaN-based light-emitting diodes with textured sidewalls and icp-transferred nanohemispherical backside reflector, IEEE Trans. Electron. Dev. 64 (9) (2017) 3672–3677.

[111] J.K. Liou, Y.C. Chan, W.C. Chen, C.H. Chang, C.Y. Chen, J.H. Tsai, W.C. Liu, Characteristics of GaN-Based LEDs with hybrid microhole arrays and SiO_2 microspheres/nanoparticles structures, IEEE Trans. Electron. Dev. 64 (7) (2017) 2854–2858.

[112] C.H. Chang, Y.L. Lee, Z.F. Wang, R.C. Liu, J.H. Tsai, W.C. Liu, Performance improvement of GaN-Based light-emitting diodes with a microhole array, 45° sidewalls, and a SiO_2 nanoparticle/microsphere passivation layer, IEEE Trans. Electron. Dev. 66 (1) (2019) 505–511.

[113] X. He, Z. Wang, Y. Pu, D. Wang, R. Tang, S. Cui, J.-X. Wang, J.-F. Chen, High-gravity-assisted scalable synthesis of zirconia nanodispersion for light emitting diodes encapsulation with enhanced light extraction efficiency, Chem. Eng. Sci. 195 (2019) 1–10.

[114] G.Y. Song, I. Jang, S.-W. Jeon, S.-H. Ahn, J.-Y. Kim, S.y. Kim, G. Sa, Controlling the surface properties of TiO_2 for improvement of the photo-performance and color uniformity of the light-emitting diode devices, J. Ind. Eng. Chem. 94 (2021) 180–187.

[115] Y. Liu, X. Wang, B. Zhang, Y. Zhou, Y. Pu, J.-X. Wang, D. Wang, J.-F. Chen, Ultrastable waterborne nanocomposite coating of polyurethane and zirconia nanoparticles to avoid rainbow effect on polyester-based superficial hardening films, Ind. Eng. Chem. Res. 63 (1) (2024) 244–251.